Visakhapatnam Chapter

Proceedings of Indian Geotechnical Conference 2020
December 17-19, 2020, Andhra University, Visakhapatnam

Predicting Residual Stress State Around Bored Cast-in-situ Piles Utilizing Cavity Contraction and Expansion Solutions

Alpha Lukose[1] and Sudheesh Thiyyakkandi[2]

[1] Research Scholar, Department of Civil Engineering, Indian Institute of Technology, Palakkad, Kerala- 678623
101704002@smail.iitpkd.ac.in

[2] Assistant Professor, Department of Civil Engineering, Indian Institute of Technology, Palakkad, Kerala- 678623
sudheesh@iitpkd.ac.in

Abstract. Deep foundations are conventionally being adopted in construction of various structures ranging from bridges to skyscrapers. Bored cast-in-situ piles and drilled shafts have become a common choice of deep foundations, especially in urban areas, owing to the relatively minimal construction associated noise and vibration as opposed to driven pile. However, one of the major shortcomings of bored piles is the lower skin and tip resistances due to the installation effects (stress relief). In the current practice, empirical or semi-empirical correlations are generally adopted for estimating the unit skin friction of bored pile/drilled shafts which is not necessarily taking into account the actual soil state around pile subsequent to the installation. Since the soil state (properties and stresses) in the vicinity of pile will be significantly altered due to the installation processes, studying the evolution of soil state during the various construction stages as well as the loading stage will aid to estimate the residual confining stress and thus the unit skin resistance of pile. This can be made possible using cavity expansion and contraction solutions as the stress relaxation during the excavation of hole is analogous to a cylindrical cavity contraction (unloading) problem and subsequent concrete placement and axial loading resemble a cavity re-loading (i.e., expansion) problem. This paper presents a semi-analytical cylindrical cavity contraction and expansion solution procedure to predict the residual horizontal stress and consequently the skin friction of bored pile. The proposed approach was validated using two well-documented field test data of bored piles/drilled shafts in sand.

Keywords: Horizontal Stress; Unit Skin Friction; Bored Piles; Drilled Shafts; Cavity Expansion and Contraction Solutions

1 Introduction

Bored piles and drilled shafts are widely used as foundation systems for buildings, bridges, transmission towers, signages, retaining structures, etc., because of their minimally invasive nature and constructability through hard strata. The skin resistance

offered by bored pile primarily depends on the residual stress state in close vicinity to the pile during the loading, which is influenced by the installation process and the behaviour of the thin layer of soil around the pile (i.e., shear band zone) upon the loading [5,11,13]. However, the existing popular methods for predicting unit skin friction such as depth-dependent β method [17], FHWA rational method [7], IS code method [9], etc., are rather empirical or semi-empirical in nature and do not consider the fundamental mechanics of the stress state evolution processes. In the recent years, advancements have been made in this direction by using numerical approaches coupled with constitutive models [11], computational algorithms [12,13], and using load transfer functions to describe pile-soil interaction [25]. Still, all these methods ignore the change in stress state caused by the method of construction (dry or wet/slurry methods).

Since the soil state in the immediate locale of the pile will be significantly altered during each stage of construction process and loading, tracking the evolution of soil state during each stage will enable more realistic prediction of residual confining stress and hence the unit skin friction of shaft. The excavation of hole and subsequent concrete placement can be considered analogous to cylindrical cavity contraction and expansion problems; and further concrete hydration and axial loading are similar to cavity contraction and expansion, respectively. A semi – analytical solution procedure, based on cylindrical cavity contraction and expansion phenomena, for predicting the residual stress state around a shaft in sand and thus its unit skin friction is presented in this paper. This solution procedure enables the full incorporation of non-linear soil behaviour during the construction and loading phases. The numerical algorithm involves discretization of the plastic zone of expanding and contracting cavities to thin cylindrical shell elements, similar to that adopted by Salgado and Randolph [19] for steady-state cavity expansion case, and an iterative approach is adopted from elastic-plastic boundary towards the cavity wall to determine the stress state and properties of each element. Unlike self-similarity technique which allows properties to be determined only at the limit /steady-state state, this solution procedure enable prediction of entire soil state at any stage of expansion or contraction. The validity of this solution approach was verified by predicting the response of two well-documented field test data of bored piles in sand.

2 Evolution of Lateral Stress around Pile

The ultimate unit shaft friction, f_s, along a bored pile in sand at a given depth, z, can be expressed as:

$$f_s = \sigma_{hf}{}' \tan\delta' = K\,\sigma_{vo}{}' \tan\delta' = \beta\,\sigma_{v0}{}' \quad (1)$$

Where, $\sigma_{hf}{}'$ - effective horizontal stress at failure; δ' - soil-shaft interface friction angle, generally assumed to be equal to the angle of internal friction of soil (ϕ'), K - coefficient of lateral earth pressure; and $\sigma_{v0}{}'$ - initial effective vertical stress. The term, $K \tan\delta'$ is collectively expressed as β [16] in all the *"β-methods"* available in literature. The effective horizontal stress at failure ($\sigma_{hf}{}'$) can be expressed as: $\sigma_{hf}{}' = \sigma_{h0}{}' + \Delta\,\sigma_h'$; where $\sigma_{h0}{}'$ is the initial effective horizontal stress and $\Delta\,\sigma_h{}'$ is the stress change due to the

installation processes (drilling, concreting and hardening) and axial loading of pile. The initial effective horizontal stress can be obtained as $\sigma'_{ho} = \left[(1-\sin\phi')OCR^{\sin\phi'}\right]\sigma'_{vo}$ [14]. The stress history of surrounding soil (i.e., variation of $\sigma_h{}'$) can be captured by modelling the entire process of bored pile construction and loading with the aid of cylindrical cavity contraction and expansion theories as illustrated in Fig. 1.

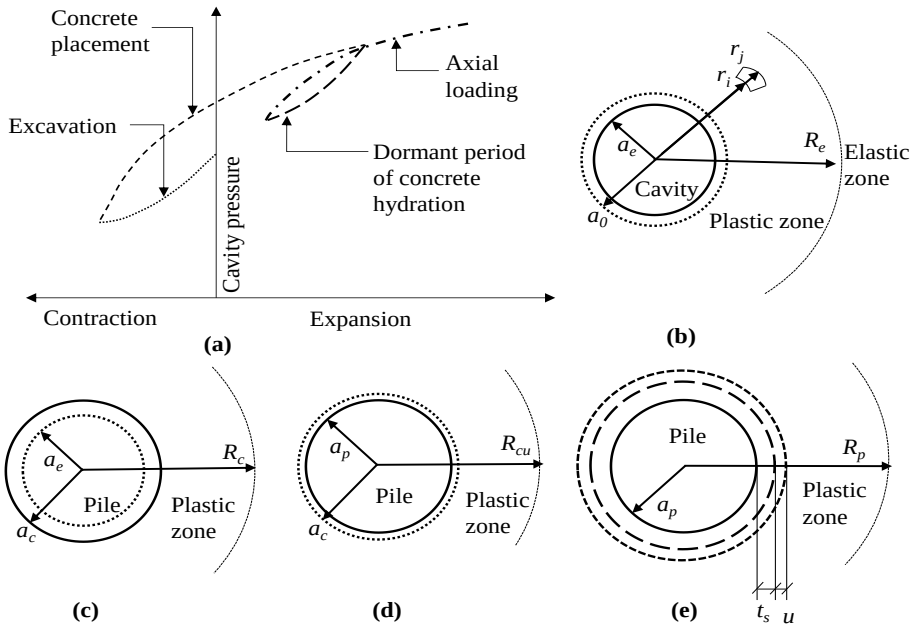

Fig. 1. Pile construction and loading – cavity contraction/expansion analogy (a) Cavity-contraction/expansion curves; (b) Excavation (contraction); (c) Concrete placement (expansion); (d) Dormant period of hydration (contraction); and (e) Axial loading

Typical cavity pressure –contraction/expansion response during the different stages of construction and axial loading is schematically depicted in Fig. 1a. During the first stage of construction, i.e., excavation of hole of radius a_0, the surrounding soil deforms inward slightly (contraction from a_0 to a_e); thus, allowing the transfer of radial stress to hoop stress around the hole through arching (Fig. 1a and 1b). The effective radial stress ($p_e{}'$) at the hole wall is given by,

$$p_e{}' = \begin{cases} 0 & \text{for dry method} \\ \gamma_b h_b & \text{for wet method, above water table} \\ \gamma_b h_b - \gamma_w h_w & \text{for wet method, below water table} \end{cases} \quad (2)$$

Where, γ_b and γ_w are the unit weight of slurry (mineral or polymer) and water, respectively; h_b is the height of slurry column above the point under consideration; and h_w is the height of water table above the point under consideration. The cavity contraction may be purely elastic or elastic-plastic with the formation of a reverse plastic zone

(radius = R_e) based on the magnitude of unloading (Fig. 1b), which depends upon the depth under consideration, location of water table, method of construction (wet or dry), etc.

The placement of fresh concrete in the shaft hole increases the lateral pressure on the cavity wall and displaces the cavity wall outward slightly (i.e., expansion from a_e to a_c; Fig. 1c) with the development of plastic zone (R_c). Though different approaches are available, predicting the lateral pressure exerted by fresh concrete is very complex as it depends on several factors such as intrinsic properties of the materials, mix proportions, consistency, slump, placement rate, length and diameter of shaft, temperature, among others [2,3,10,21]. Lings et al. [10] found that variation of lateral concrete pressure with depth is in conformity with the fluid concrete hydrostatic line down to certain depth, known as critical depth ($h_{cr} \approx \frac{1}{3} \times$ depth of excavation), below which it follows the slope of slurry pressure line. Accordingly, lateral pressure (p_c) exerted on the wall at a depth (z) immediately after the concrete placement can be obtained as:

$$p_c = \begin{cases} \gamma_c \, z & \text{for } z \leq h_{cr} \\ (\gamma_c - \gamma_b) h_{cr} + \gamma_b \, z & \text{for } z > h_{cr} \end{cases} \quad (3)$$

For the location below water table, effective lateral pressure, $p_c' = p_c - \gamma_w h_w$.

It has been reported by several researchers [1-5,10] that concrete lateral pressure decreases with time during the hydration of concrete. This is attributed to the physical restructuring of solid particles (thixotropy) and the increase of internal friction as well as the autogenous and drying shrinkage effects [2,3,5]. The drop in lateral pressure during the plastic stage of cement hydration (i.e., dormant period) is reported to be predominantly due to the physical effect, which is related to the coarse aggregate concentration in concrete [2,3]. This drop in lateral concrete pressure causes cavity contraction (from a_c to a_p) and decreases the horizontal stresses around the pile (Fig. 1d). By the end of dormant period, the concrete skeleton becomes relatively rigid [2,3] and further contraction during the accelerated stage of cement hydration (i.e., after dormant period) is expected to be negligible even though the internal pressure within concrete drop to zero. Assaad and Khayat [2] have observed a concrete pressure drop of 40 - 50% during the dormant period in their experimental study.

Finally, during the axial loading phase, shear strains develop in soil surrounding the shaft owing to the vertical displacement of the shaft [7,11]. These shear strain tend to be prevalent within a thin cylindrical shear band of thickness, t_s, formed around the pile, which depends upon the soil gradation; typically, in the range of 5-20 times the mean grain size, D_{50} [21,22]. During the loading, the pile and shear band is considered together as an indefinite cylinder with initial radius ($r_{pf} = a_p + t_s$), which undergoes a radial expansion/displacement of u that depends on the dilation potential of the soil (Fig. 1e). The magnitude of this radial displacement (u) is given by [13]:

$$u = t_s \tan\psi' \frac{\gamma_{cs}}{2} \quad (4)$$

Where, ψ' is the dilation angle of soil and γ_{cs} is the shear strain to attain critical state.

During the axial loading, as the shear band expands, the surrounding soil deforms elastically until the onset of plastic yielding at the cavity wall (r_{pf}) and beyond that, a plastic zone is formed around the cavity, the radius of which (R_p) increases with further loading (Fig.1e). The maximum radial stress generated at the outer boundary of shear band during the loading stage, which is influenced by the residual soil state subsequent to the pile installation, governs the ultimate unit skin resistance of pile at that depth. The proposed cavity contraction and expansion solutions procedure for the same is described below.

3 Cylindrical Cavity Contraction and Expansion Solutions

3.1 Equilibrium Equation, Yield Criterion, and Flow Rule

The stress equilibrium around a cylindrical cavity can be expressed as:

$$\frac{d\sigma_r{}'}{dr} + \frac{\sigma_r{}' - \sigma_\theta{}'}{r} = 0 \tag{5}$$

Where, σ_r' and σ_θ' are the effective radial and hoop stresses. It is assumed that pore water pressure (p_w) remains constant throughout the installation and loading; i.e., $\frac{dp_w}{dr} = 0$. The conventional geomechanics sign convention of compressive stresses and strains as positive is adopted here. The Mohr-Coulomb yield criteria for loading and unloading are given by Eqs. (6) and (7), respectively.

$$\sigma_r{}' = \sigma_\theta{}' N \tag{6}$$

$$\sigma_\theta{}' = \sigma_r{}' N \tag{7}$$

Where, N is the flow number; $N = \frac{1+\sin\phi'}{1-\sin\phi'}$. The friction angle ($\phi'$) of soil within the plastic zone of an expanding and contracting cavity vary with the volumetric plastic strain, which is assumed to vary according to the Bolton (1986) model [6] for sand:

$$\phi_{ij}{}' = \phi_c{}' + D_\psi \left\{ I_{D_{ij}} \left[Q + \ln\left(\frac{p_a}{100\, p_{ij}{}'} \right) \right] - R_Q \right\} \tag{8}$$

Where, $\phi_{ij}{}'$ is the friction angle within a thin shell element, ij (Fig. 1b); $\phi_c{}'$ is the critical state friction angle; $I_{D_{ij}}$ is the relative density within element, ij; p_a is the reference stress = 100 kPa; Q and R_Q are fitting parameters ($Q \approx 10$ and $R \approx 1$); $p_{ij}{}'$ is the mean effective stress within element, ij; and D_ψ = 3 for triaxial test and 5 for plane strain test. The dilatancy (ψ_{ij}') and friction angles are assumed to hold the relationship given by Bolton [6]:

$$\psi_{ij}{}' = \frac{\phi_{ij}{}' - \phi_c{}'}{0.8} \tag{9}$$

A non–associated flow rule proposed by Zhang and Salgado [24] for Mohr-Coulomb soils is assumed to hold true:

$$N_{ij} = N_c D_{ij} \tag{10}$$

Where, N_{ij} is the flow number within element, ij; N_c is critical state flow number; and D_{ij} is the strain rate ratio within ij given by:

$$D_{ij} = 1 - \left(\frac{\dot{\varepsilon_v}}{\dot{\varepsilon_1}}\right) \tag{11}$$

Where, $\dot{\varepsilon_v}$ is the volumetric strain rate = $\varepsilon_v{}^{(i)} - \varepsilon_v{}^{(j)}$ and $\dot{\varepsilon_1}$ is the major principal strain rate = $\varepsilon_1{}^{(i)} - \varepsilon_1{}^{(j)}$; for expansion, $\dot{\varepsilon_1} = \dot{\varepsilon_r}$ and for contraction, $\dot{\varepsilon_1} = \dot{\varepsilon_\theta}$. The strain components are defined as logarithmic strains to account for large strain in the plastic zone:

$$\left.\begin{aligned} \varepsilon_r^{(i)} = -ln\left(\frac{r_j - r_i}{(r_j - u_j) - (r_i - u_i)}\right); \quad \varepsilon_\theta^{(i)} = -ln\left(\frac{r_i}{r_i - u_i}\right); \\ \varepsilon_v^{(i)} = -ln\left(\frac{r_j^2 - r_i^2}{(r_j - u_j)^2 - (r_i - u_i)^2}\right) \end{aligned}\right\} \tag{12}$$

3.2 Numerical solution procedure

For obtaining the evolution of soil state during the various stages of bored pile construction and loading, which will aid to estimate the residual confining stress around pile, an elaborate numerical procedure is adopted and is briefed below:

(i) Select required input parameters: a_0, $p_0' = \sigma_{h0}'$, I_{D0}, ϕ_c', t_s, γ_{cs}, and shear modulus, G.

Excavation of Shaft Hole. When the internal pressure decreases from p_0', unloading happens; which will be purely elastic until reverse yielding occurs. The cavity pressure at the beginning of reverse yielding (p_r') is:

$$p_r{}' = \frac{p_0{}'(N+1)}{N(N+1)} \tag{13}$$

(ii) If the effective radial stress after excavation (p_e') is greater than p_r', the corresponding contracted cavity radius (a_e) and radial and hoop stress fields around the cavity can be calculated as:

$$a_e = a_0\left(1 + \frac{(p_e{}' - p_0{}')}{2G}\right) \tag{14}$$

$$\sigma_r{}' = p_0{}' + (p_e{}' - p_0{}')\left(\frac{a_e}{r}\right)^2; \quad \sigma_\theta{}' = p_0{}' - (p_e{}' - p_0{}')\left(\frac{a_e}{r}\right)^2 \tag{15}$$

If $p_e' < p_r'$, the plastic unloading happens and a reverse plastic zone forms around the cavity. The accurate determination of stress and strain fields around the cavity considering the effect of volumetric plastic strain requires cavity radius (a_e) or the plastic radius (R_e) be known. However, since both a_e and R_e are initially unknown, a recursive approach with the assumed plastic radius is adopted to obtain the actual a_e and R_e and thus to estimate the variation of soil properties and stress state within the plastic zone concurrently. For each assumed plastic radius, plastic zone is discretized into thin elements and an iterative approach beginning from the elastic-plastic boundary is employed as summarized below:

(iii) Assume a reverse plastic radius, R_{e1}. Divide this plastic zone into thin shell elements (ij), each of thickness dr, where j marks the outer boundary of each element. The first element is considered close to boundary with inner radius, $r_i = r_j - dr$ and outer radius, $r_j = R_{e1}$, where the entire soil state is known:

$$\left.\begin{array}{c} {\sigma_{r_j}}' = \ {p_r}' = \ {\sigma_R}' ; \quad {\sigma_{\theta_j}}' = \ {\sigma_R}' . N_p \\ \varepsilon_r^{(j)} = \ -({p_0}' - \ {\sigma_R}') \ / \ 2G; \ \ \varepsilon_\theta^{(j)} = -\varepsilon_r^{(j)} \\ \varepsilon_v^{(j)} = \varepsilon_r^{(j)} + \ \varepsilon_\theta^{(j)} \ \text{and} \ \ u_j = \ \varepsilon_\theta^{(j)} . R_{e1} \end{array}\right\} \tag{16}$$

The friction angle of this first element (ϕ_{ij}') is considered same as that at r_j for initial iteration and then:

- Determine the inner radial stress (${\sigma_{r_i}}'$) using Eq. (17), which is obtained by combining Eqs. (5) and (7). Subsequently, determine inner hoop stress (${\sigma_{\theta_i}}'$) using Eq. (7) and mean stress (${p_{ij}}'$) for the element by Eq. (18), obtained by modifying Davis (1968) equation [8] to apply for the unloading case.

$${\sigma_{r_i}}' = \ {\sigma_{r_j}}' . \ \left(\frac{r_j}{r_i}\right)^{(1-N_{ij})} \tag{17}$$

$${p_{ij}}' = \frac{1}{3} . \ \left[\bar{\sigma}_r \ (1 + N_{ij})(1 + \mu_{ij}) \right] \tag{18}$$

Where, $\bar{\sigma}_r$ - average radial stress for the element and μ_{ij} = 0.5 (1+ $\sin \phi_{ij}' . \sin \psi_{ij}'$).

- By substituting Eq. (12) in Eq. (11), an expression with inner radial displacement, u_i as the only unknown is obtained (Eq.19), where D_{ij} is obtained from Eq. (10). Solve Eq. (19) for u_i using numerical method (e.g., Newton Raphson method).

$$\varepsilon_v^{(j)} + \left(D_{ij} - 1\right)\varepsilon_\theta^{(j)} = \ln\left\{\left[\frac{\left(r_j - u_j\right)^2 - (r_i - u_i)^2}{{r_j}^2 - \ {r_i}^2}\right] . \ \left[\frac{r_i \ - u_i}{r_i}\right]^{\left(D_{ij} \ -1\right)}\right\} \tag{19}$$

- Estimate the radial, hoop, and volumetric strains ($\varepsilon_r^{(i)}$, $\varepsilon_\theta^{(i)}$ and $\varepsilon_v^{(i)}$) using Eq. (12). Subsequently, using $\varepsilon_v^{(i)}$, calculate a new void ratio (e_{ij}) and hence relative density ($I_{D_{ij}}$) of the element from which the new ϕ_{ij}' can be obtained using Eq. (8).

- The above steps are iterated to obtain sufficient convergence for ϕ_{ij}'. All the parameters at inner boundary *'i'* will be thus obtained, which will be the outer boundary (*j*) for the next element inwards.

(iv) Repeat Step (iii) for the next element and proceed element by element inwards. After achieving convergence for each element, $r_i - u_i$ is compared with the initial cavity radius (a_0). If $r_i - u_i > a_0$, carry forward with the next element; whereas, if $r_i - u_i \approx a_0$, cavity wall has been reached.

(v) Check if the difference between estimated cavity stress, σ_{r_i}' and p_e' (Eq. 2) is satisfactorily small. If not, repeat the above Steps (iii and iv) by gradually incrementing the plastic radius as R_{e2}, R_{e3}, …, R_{en} until $\sigma_{r_i}' \approx p_e'$. This iterative procedure will simultaneously give the stresses, strains and the varied soil properties within the plastic zone corresponding to the effective cavity pressure of p_e'.

Concrete placement. Cavity expansion resulting from concrete placement is considered here. The effective lateral pressure immediately after the concrete placement (p_c') will certainly exceed the minimum pressure to cause plastic yielding $\left(p_y' = \frac{p_e'(N+1)}{N(N+1)}\right)$. The numerical procedure followed is similar to that adopted for plastic contraction and is summarized below:

(vi) Consider a plastic radius, R_{c1}, greater than a_e. Divide this plastic zone into thin shell elements (*ij*), each with thickness *dr*.

(vii) The stresses, strains and radial displacement values (σ_R', σ_θ', ε_R, ε_θ and u_R) at R_{c1} can be determined using Eq. (20) as follows:

$$\left.\begin{array}{c} \sigma_R' = \dfrac{2\,N\;\sigma_{re}'}{1+N};\; \sigma_\theta' = \dfrac{\sigma_R'}{N}\;;\; \varepsilon_R = \dfrac{\sigma_R' - \sigma_{re}'}{2G} \\ \varepsilon_\theta = -\,\varepsilon_R;\;\; u_R = -\,\varepsilon_\theta\,.\;R_{c1} \end{array}\right\} \qquad (20)$$

Where, σ_{re}' and N are the radial stress and flow number at R_{c1} following excavation.

(viii) The first element (*ij*) is considered with the outer boundary $r_j = R_{c1}$ and ϕ_{ij}' of the element is initially assumed to be the same as that at R_{c1} at the end of excavation phase.

- Determine σ_{r_i}' utilizing Eq. (21) (obtained by combining Eqs. 5 and 6), σ_{θ_i}' using Eq. (6) and p_{ij}' by Eq. (22); Davis (1968) equation [8,19]:

$$\sigma_{r_i}' = \sigma_{r_j}' \left(\frac{r_j}{r_i}\right)^{\frac{N_{ij}-1}{N_{ij}}} \qquad (21)$$

$$p_{ij}' = \frac{1}{3}\left[\bar{\sigma}_r \left(1 + \frac{1}{N_{ij}}\right)(1 + \mu_{ij})\right] \qquad (22)$$

- Obtain u_i by solving Eq. (23); derived by plugging Eq. (12) in Eq. (11).

$$\varepsilon_v^{(j)} + \left(D_{ij} - 1\right)\varepsilon_r^{(j)} = \ln\left\{\left[\frac{\left(r_j - u_j\right)^2 - (r_i - u_i)^2}{{r_j}^2 - {r_i}^2}\right] . \left[1 + \frac{u_i - u_j}{r_j - r_i}\right]^{(D_{ij}-1)}\right\} \quad (23)$$

- Estimate the radial, hoop and volumetric strains ($\varepsilon_r^{(i)}$, $\varepsilon_\theta^{(i)}$ and $\varepsilon_v^{(i)}$) using Eq. (12). Subsequently, using $\varepsilon_v^{(i)}$, calculate a new void ratio (e_{ij}) and hence relative density ($I_{D_{ij}}$) of the element from which the new ϕ_{ij}' can be obtained using Eq. (8).

- The above steps are iterated to obtain sufficient convergence for ϕ_{ij}'. This iterative process yields all the parameters at the inner face of the element (i).

(ix) Go to the next element and follow Step (viii). Once convergence is achieved for each element, r_i - u_i is compared with a_e. If $r_i - u_i > a_e$, proceed to the next element. If $r_i - u_i \approx a_e$, cavity wall has been reached and corresponding new cavity radius, $a_c = r_i$.

(ix) Compare the computed cavity pressure (σ_{ri}') with p_c' (Eq. 3); if the difference is not adequately small, repeat the above steps by increasing the plastic radius in small increments (R_{c2}, R_{c3}...., R_{cn}) until the close agreement is achieved. Corresponding to p_c', the distribution of stresses, strain, and soil properties within the plastic region will be known.

Plastic phase of Concrete hydration. Drop of pressure during the dormant period of concrete hydration will cause inward deformation of the surrounding soil (i.e., cavity radius reduces from a_c to a_p). The variation of stresses and strains with the radial distance at the end of pressure drop can be obtained using the procedure adopted for excavation.

Axial loading. During axial loading, the pile and shear band is considered to form a cylindrical cavity with initial radius ($r_{pf} = a_p + t_s$), which will be displaced through a radial distance, u (Eq. 4). The procedure adopted for modelling the concrete placement can be utilized here to obtain the soil state (stresses, strains, and soil properties) corresponding to the full expansion of shear band.

4 Results and Discussions

4.1 Comparison with the Experimental Results

Two well-documented field load test results of bored pile /drilled shaft were utilized for the validation of the proposed approach. A shear band thickness (t_s) of $5D_{50}$ was adopted for the prediction. Unit weight for bentonite slurry and concrete was assumed as 10.1 kN/m^3 and 24 kN/m^3, respectively. A pressure drop of 50 % during the dormant period of concrete hydration is assumed here [2]. The first case is an axial load test data on drilled shaft (TS2; length, L = 5.5 m and diameter, D = 1.22 m) in typical Florida sand reported by Thiyyakkandi et al. [20]. The soil in test site was predominantly sand with silt (SP-SM) with a thin layer of clay (0.75 m) on top. The water table at the time of load testing was 1.8 m below the ground surface. The β profile for the shaft was

produced by the proposed approach using the following input parameters [15,20]: D_{50} = 0.16 – 0.2 mm; e_{max} = 0.80; e_{min} = 0.43; G (kPa) = 8000 + 650.z (z- depth; estimated from pressuremeter test); γ_{cs} = 160%; top sand layer (0.75 – 3.80 m): ϕ_c' = 31^0, I_{D0} = 40% and bottom sand layer (3.80 – 5.50 m): ϕ_c' = 34^0, I_{D0} = 50%. Figure 2a displays the experimental and predicted β values (for D_{50} of 0.16 mm and 0.2 mm).

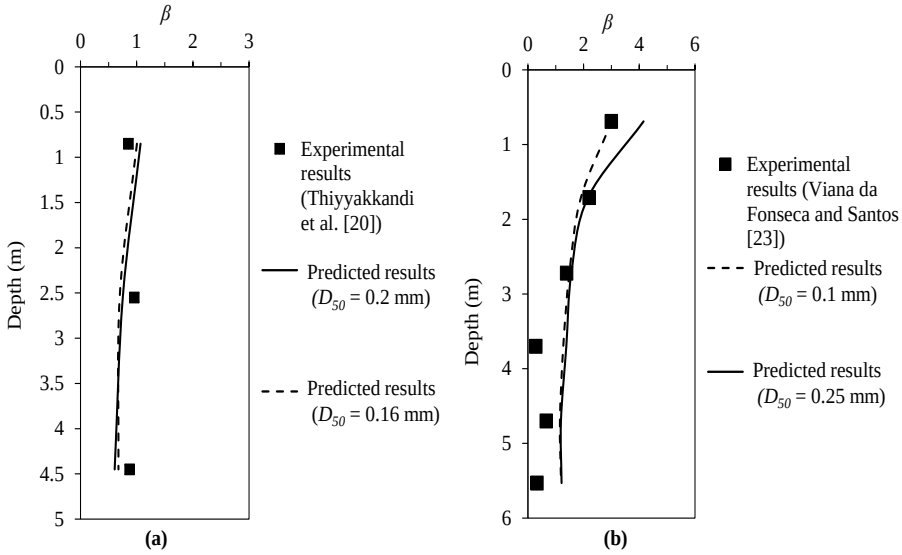

Fig. 2. Comparison of predicted vs. experimental β values (a) Thiyyakkandi et al. [20]; (b) Viana da Fonseca and Santos [23]

The second case is a bored pile load test data reported by Viana da Fonseca and Santos [23]. The pile (L = 6 m and D = 0.6 m) was bored in saprolitic granite soil, which extended up to 20 m below the ground surface. The water table was located 10 m below the ground surface. The soil parameters considered for the prediction are as follows [13,23]: D_{50} = 0.10 – 0.25 mm; G_0 (MPa) = 120 + 5.z; G = 0.5 G_0; γ_{cs} = 60%; ϕ_c' = 32^0, I_{D0} = 40%; e_{max} ≈ 0.90 and e_{min} ≈ 0.60 (estimated from D_{50} using the correlations proposed by Patra et al. [18]). The comparison between the predicted β profiles (for D_{50} = 0.10 mm and 0.25 mm) and experimental results is shown in Fig. 2b. It can be seen from Fig. 2 that the predicted range of β values are consistent with the experimental data, except some deviation in second case and this signifies good predictive capability of the presented approach.

4.2 Stress distribution around shaft

Figure 3 shows the predicted stress state around Shaft TS2 [20], at a depth of 2.55 m. The stress state around the pile at different stages of installation and testing can be effectively predicted as shown. The different stages considered are: (a) in-situ k_0 condition; (b) excavation of shaft hole stabilized using bentonite slurry; (c) concrete placement; (d) plastic stage of concrete hydration; and (e) axial load test.

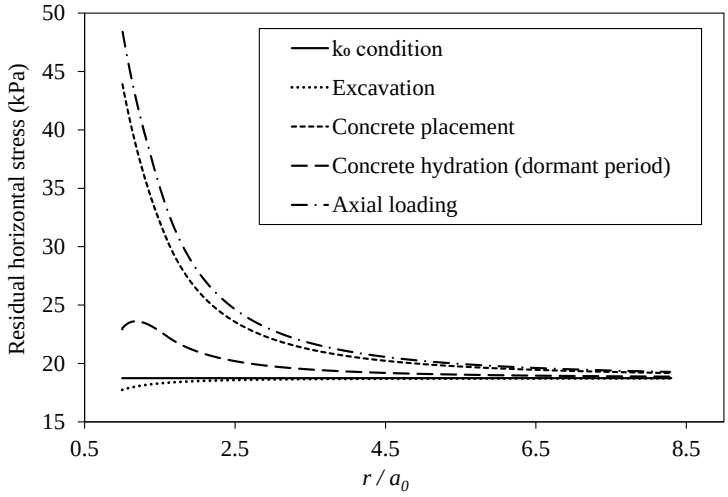

Fig.3. Residual horizontal stress around a shaft at different stages of pile installation and loading (for Shaft TS2 at 2.55 m depth; Thiyyakkandi et al. [20])

5 Conclusion

This paper has presented a semi-analytical approach in the framework of cavity contraction and expansion theories for tracking the evolution of stress state around a drilled shaft / bored pile during different stages of construction and axial loading. Unlike the existing self-similarity-based techniques, the presented solution enables prediction of soil state at any stage of expansion/contraction, incorporating the effect of volumetric plastic strain on the soil properties and stresses, throughout the plastic zone. The state of soil around a pile, which is significantly altered by the installation processes (excavation, concrete placement, and hydration) as well as the loading, could be captured using the presented method. The predictive capability of this solution method was validated by reproducing the two well-documented experimental results on drilled shafts / bored piles.

References

1. Alexandridis, A., & Gardner, N. (1981). Mechanical behaviour of fresh concrete. Cement and Concrete Research, 11(3), 323-339.
2. Assaad, J. J., & Khayat, K. H. (2006). Effect of mixture consistency on formwork pressure exerted by highly flowable concrete. Journal of materials in civil engineering, 18(6), 786-791.
3. Assaad, J., & Khayat, K. H. (2004). Variations of lateral and pore water pressure of self-consolidating concrete at early age. *ACI Materials Journal*, *101*(4), 310-317.
4. Assaad, J., Khayat, K. H., & Mesbah, H. (2003). Variation of Formwork Pressure with thixotropy of Self-Consolidating Concrete. *ACI Materials Journal*, *100*(1), 29-37.

5. Bernal, J. B., & Reese, L. C. (1983). *Study of the lateral pressure of fresh concrete as related to the design of drilled shafts.* No. FHWA/TX-84/45+ 308-lF, University of Texas at Austin., Center for Transportation Research.
6. Bolton, M. D. (1986). The strength and dilatancy of sands. *Geotechnique, 36*(1), 65-78.
7. Brown, D. A., Turner, J. P., Castelli, R. J., & Americas, P. B. (2010). *Drilled shafts: Construction procedures and LRFD design methods.* United States. Federal Highway Administration.
8. Davis, E. H. (1968). Theories of Plasticity and Failure of Soil Masses. In I. K. Lee., *Chapter 6, Soil-Mechanics—Selected Topics* (pp. 341-380). London: Butterworths.
9. IS 2911(Part 1 / Sec 2). (2010). *Design and construction of pile foundations.* Bureau of Indian Standards, New Delhi.
10. Lings, M. L., Ng, C. W., Nash, D. F., & 108., C. R. (1994). The lateral pressure of wet concrete in diaphragm wall panels cast under bentonite. *107*(3), 163-172.
11. Loukidis, D., & Salgado, R. (2008). Analysis of the shaft resistance of non-displacement piles in sand. *Geotechnique, 58*(4), 283-296.
12. Mascarucci, Y., Miliziano, S., & Mandolini, A. (2014). A numerical approach to estimate shaft friction of bored piles in sands. *Acta Geotechnica, 9*(3), 547-560.
13. Mascarucci, Y., Miliziano, S., & Mandolini, A. (2016). 3M analytical method: evaluation of shaft friction of bored piles in sands. *Journal of Geotechnical and Geoenvironmental Engineering, 142*(3), 04015086.
14. Mayne, P. W., & Kulhawy, F. H. (1982). Ko- OCR Relationships in Soil. *Journal of the Soil Mechanics and Foundations Division, 108*(6), 851-872.
15. McVay, M., Bloomquist, D., & Thiyyakkandi, S. (2014). *Field Testing of Jet-Grouted Piles and Drilled Shafts (BDK75-977-41).* Tallahassee, FL.: Final report submitted Florida Department of Transportation.
16. Meyerhof, G. G. (1976). Bearing capacity and settlement of pile foundations. *J. Geotech. Eng. Div., 102*(GT3), 197–228.
17. O'Neill, M., & Hassan, K. (1994). Drilled Shafts: Effects of construction on performance and design criteria. *Proc., Int. Conf. Des. Constr. Deep Founds. Orlando, FHWA, 1.*
18. Patra, C., Sivakugan, N., & Das, B. (2010). Relative density and median grain-size correlation from laboratory compaction tests on granular soil. *International journal of geotechnical engineering, 4*(1), 55-62.
19. Salgado, R., & Randolph, M. (2001). Analysis of cavity expansion in sand. *International Journal of Geomechanics , 1*(2), 175-192.
20. Thiyyakkandi, S., McVay, M., Lai, P., & Herrera, R. (2016). Full-scale coupled torsion and lateral response of mast arm drilled shaft foundations. *Canadian Geotechnical Journal, 53*(12), 1928-1938.
21. Uesugi, M., Kishida, H., & Tsubakihara, Y. (1988). Behavior of sand particles in sand-steel friction. *Soils and foundations, 28*(1), 107-118.
22. Vardoulakis, I., & Sulem, J. (1995). *Bifurcation analysis in geomechanics.* London: Blackie Academic and Professional.
23. Viana da Fonseca, A., & Santos, J. (2008). *Behaviour of CFA, Driven and Bored Piles in Residual Soil. International Prediction Event-Experimental Site-ISC'2.* FEUP/IST, Portugal.
24. Zhang, J., & Salgado, R. (2010). Stress-dilatancy relation for Mohr-Coulomb soils following a non-associated flow rule. *Geotechnique, 60*(3), 223-226.
25. Zhang, Q.-q., Feng, R.-f., Yu, Y.-l., Liu, S.-w., & Qian, J.-g. (2019). Simplified approach for prediction of nonlinear response of bored pile embedded in sand. *Soils and Foundations, 59*(5), 1562-1578.